Polymer Chemistry

ROYAL SOCIETY OF CHEMISTRY

PAPER

View Article Online
View Journal | View Issue

Cite this: *Polym. Chem.*, 2025, **16**, 3138

Tuning the properties of polysulfides using functionalised cardanol crosslinkers†

Mahsaalsadat Rokni, [a,b] Manon Lambert[a,c] and Erin M. Leitao *[a,b]

This study presents the synthesis, characterisation, and property analysis of surface-functionalised polysulfides synthesised *via* inverse vulcanisation of elemental sulfur with cardanol and its silane-functionalised derivatives. Three polysulfide formulations, poly-(S-*r*-C), poly-(S-*r*-C_{APS}), and poly-(S-*r*-C_{TMS}), were prepared to investigate the impact of functional groups on the crosslinked polysulfide's properties. Reacting the cardanol hydroxy group with either 3-aminopropyltriethoxysilane (APTES) or chlorotrimethylsilane (TMS) enabled the modification of the polysulfide networks. Characterisation, including NMR spectroscopy, FTIR spectroscopy, SEM, contact angle measurements, thermogravimetric analysis (TGA), differential scanning calorimetry (DSC), and ASTM D3359 cross-hatch adhesion testing, was conducted. Poly-(S-*r*-C) and poly-(S-*r*-C_{APS}) demonstrated strong adhesion to glass substrates and higher thermal stability, attributed to hydrogen bonding and the formation of Si–O–Si networks, respectively. In contrast, poly-(S-*r*-C_{TMS}), bearing nonpolar trimethylsilyl groups, exhibited weaker adhesion and lower thermal residue. The results highlight how chemical functionality governs adhesion, wettability, solubility, and thermal behavior. This work demonstrates the potential of renewable cardanol-based monomers in designing sustainable sulfur-rich materials for applications in coatings and adhesives.

Received 14th May 2025,
Accepted 10th June 2025

DOI: 10.1039/d5py00478k

rsc.li/polymers

Introduction

Growing environmental concerns over the reliance on petroleum-based materials have driven the search for sustainable alternatives with comparable or superior properties. In this regard, sulfur-rich polymers, polysulfides, have emerged as promising materials, offering mechanical strength, thermal stability, and adhesive properties that make them valuable for coatings, adhesives, and other functional materials.[1–3] A key approach to making these materials more sustainable is to use crosslinkers derived from renewable resources. By incorporating naturally occurring compounds functionalised with reactive groups, such as alcohols and alkenes, polymerisation with sulfur to generate polysulfides with tunable properties, is possible. Inverse vulcanisation, a process in which elemental sulfur polymerises with alkene-containing monomers, has proven to be an effective method for producing chemically stable, processable sulfur-rich polymers with adjustable thermomechanical properties (Scheme 1).[4–13] Beyond the dynamic and adaptable nature of the polysulfides, the monomers can be functionalised to fine-tune surface chemistry and performance, enabling applications in advanced materials, environmental systems, and energy technologies.[14,15]

Previous studies using crosslinkers containing hydroxyl groups (Scheme 1a–c), such as perillyl alcohol (a)[16] and farne-

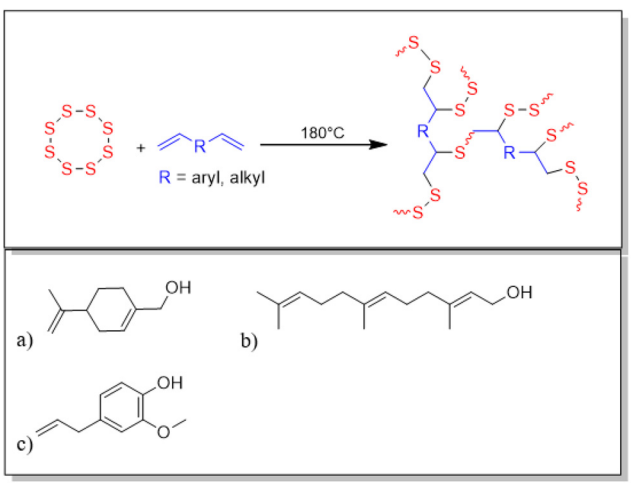

Scheme 1 General reaction scheme of inverse vulcanisation (top) and selected examples of previously used crosslinkers (bottom): (a) perillyl alcohol, (b) farnesol, (c) eugenol.

[a]*School of Chemical Sciences, University of Auckland, 1010, New Zealand. E-mail: erin.leitao@auckland.ac.nz*
[b]*The MacDiarmid Institute for Advanced Materials and Nanotechnology, New Zealand*
[c]*Polytech Université Claude Bernard, Lyon, France*

† Electronic supplementary information (ESI) available. See DOI: https://doi.org/10.1039/d5py00478k

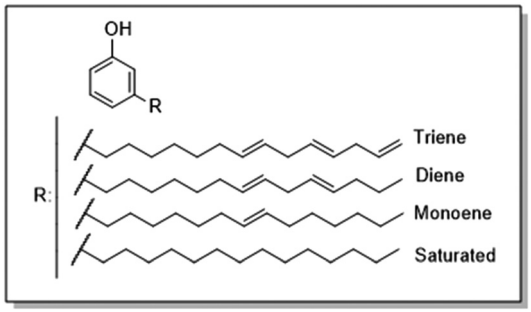

Scheme 2 Structural variants of cardanol based on side-chain unsaturation.

sol (b)[3,17] have shown that primary alcohols may undergo side reactions, including the loss of the hydroxyl group during sulfur polymerisation. In contrast, crosslinkers bearing phenolic hydroxyl groups, such as eugenol (c), have demonstrated retention of the hydroxyl group after polymerisation.[18] Based on these reports, for our study, we chose the crosslinker cardanol, a renewable phenolic compound derived from cashew nuts. Cardanol is not a single defined molecule but a mixture of phenolic lipids with a C15 side chain exhibiting varying degrees of unsaturation. Its composition typically includes saturated, mono-, di-, and tri-unsaturated components, and can vary depending on the source and extraction method (Scheme 2).[19] Cardanol provides (1) a phenolic hydroxyl group which survives the inverse vulcanisation process and is available for facile modification, (2) sufficient separation between the hydroxyl and alkene functionalities to maintain hydrophilic and hydrophobic domains in the polysulfide. Its inherent flexibility and chemical reactivity make it an excellent candidate for modifying polysulfides. In addition, phenolic compounds have been reported to participate in radical polymerization by acting as hydrogen atom donors, potentially functioning as chain transfer agents and influencing polymer growth dynamics.[20,21] By introducing polar (amine, hydroxyl) and nonpolar (silane) functionalities through cardanol derivatisation, our aim was to tailor the properties of the crosslinked polysulfides. Cardanol derivatisation was possible through reactions with 3-aminopropyltriethoxysilane (APTES) and chlorotrimethylsilane (TMSCl).[22,23] This strategy contributes to the development of sustainable polymers with interesting adhesion properties, wettability, thermal stability, mechanical strength, and chemical durability.

Experimental

Materials

Sulfur (S_8 powder, Riedel-de Haen), cardanol (Combi-Blocks, Inc.), chloroform-D ($CDCl_3$, Cambridge Isotope Laboratories Inc.), ethanol (ECP Limited), 3-aminopropyltriethoxysilane (APTES) and chlorotrimethylsilane (Sigma-Aldrich), triethylamine (TEA) (JT Baker), and ethyl acetate (Honeywell). All materials were used as received.

Instrumentation

For ^1H, ^{13}C NMR spectroscopy, samples were dissolved in $CDCl_3$ and run on a Bruker Avance 400 MHz spectrometer, with spectra recorded in parts per million (ppm). Tetramethylsilane (TMS) was used for calibration, and residual protium in NMR solvents provided a reference (7.26 ppm for $CDCl_3$). $CDCl_3$ (77.3 ppm) was used to reference $^{13}C\{^1H\}$ NMR spectra. The data processing was carried out using Bruker TopSpin® software. Fourier-transform infrared spectroscopy (FT-IR) data were acquired using a Bruker Vertex70, between 400 cm^{-1} to 4000 cm^{-1}.

Gel permeation chromatography (GPC) was used to measure molecular weight distributions. The instrument, equipped with three PS-DVB columns (Shimadzu, Shim-pack GPC-801), was run at 50 °C through a refractive index detector. THF was used to dissolve samples which were then filtered using a 22 μm PTFE filter and the eluting flow rate was set to 0.5 mL min^{-1}, with the calibration curve made using polystyrene standards with narrow polydispersity. All GPC samples were run in triplicate with outliers being excluded.

Differential Scanning Calorimetry (DSC) results were obtained using a TA Instrument Q1000 DSC, under nitrogen flow, with heating from −80 °C to 150 °C with heating rate of 10 °C min^{-1} and cooling rates of 5 °C min^{-1}. Thermogravimetric analysis (TGA) was performed using a TA Instrument Q500, heating samples to 700 °C under nitrogen at a rate of 10 °C min^{-1}.

The spin coating was performed using a Laurell Technologies Corporation machine, the model is WS-650MZ-23NPP. Scanning electron microscopy (SEM) and energy-dispersive X-ray spectroscopy (EDX) analysis was updated to use a Hitachi SU-70 Schottky field emission scanning electron microscope, with specimens sputter-coated with platinum (Pt) for 60 seconds using a Hitachi E-1045 ion sputter. Contact angle measurements were performed with a Biolin Scientific Theta Lite instrument.

Synthesis of cardanol-APS (C_{APS})

APTES (3.54 g, 20.0 mmol) was first hydrolysed by dissolving it in ethanol (20 mL), followed by the dropwise addition of water (1.08 mL, 60.0 mmol, 3 equivalents). The solution was stirred at room temperature for 1 hour. Cardanol (6.00 mL, 5.45 g, 18.0 mmol) was then added directly to the hydrolysed solution, and the mixture was refluxed at 120 °C in excess ethanol for 7 hours to promote condensation between silanol and hydroxyl groups. After completion, the solvent was removed under reduced pressure to obtain the product.

Synthesis of cardanol-TMS (C_{TMS})

In a nitrogen-purged Schlenk flask, cardanol (6.00 mL, 5.45 g, 18.0 mmol) was added and maintained under a nitrogen atmosphere. Chlorotrimethylsilane (3.00 mL, 23.6 mmol, 1.3 equivalents) was introduced, followed by triethylamine (2.50 mL, 18.0 mmol, 1 equivalent) and ethyl acetate (20 mL) as the reaction medium. The mixture was stirred for 1 hour,

then filtered to remove triethylammonium chloride ($Et_3N{\cdot}HCl$). The filtrate was dried to remove residual triethylamine and ethyl acetate, yielding the desired cardanol-TMS product.

Synthesis of poly-(S-*r*-C)

To a 20 mL glass vial equipped with a magnetic stirrer, elemental sulfur (0.5023 g, 1.96 mmol, 1.16 equiv.) was added and heated to 180 °C until fully melted. Cardanol (0.5026 g, 1.68 mmol, 1.0 equiv.) was then added under stirring at 550 rpm. The mixture was stirred at 180 °C for 45 minutes, during which it darkened and reached its vitrification point. The polymer was cooled to room temperature, washed with water, and dried in an oven.

Synthesis of poly-(S-*r*-C_{APS})

To a 20 mL glass vial equipped with a magnetic stirrer, elemental sulfur (0.5012 g, 1.95 mmol, 1.84 equiv.) was added and heated to 180 °C until melted. Cardanol-APS (0.5041 g, 1.06 mmol, 1.0 equiv.) was then added under stirring at 550 rpm. The reaction was continued for 10 minutes until vitrification occurred. The light brown solid was cooled to room temperature, washed with water, and dried in an oven.

Synthesis of poly-(S-*r*-C_{TMS})

A 20 mL glass vial was equipped with a magnetic stirrer and charged with elemental sulfur (0.5023 g, 1.96 mmol, 1.45 equiv.), which was heated to 180 °C until fully melted. Cardanol-TMS (0.5000 g, 1.35 mmol, 1.0 equiv.) was then added under stirring at 550 rpm. The mixture was stirred for 45 minutes at 180 °C until it reached vitrification. The polymer was allowed to cool, washed with water, and dried in an oven.

Results and discussion

Synthesis and characterisation of cardanol functionalised crosslinkers

Cardanol (C), and two synthesised cardanol derivatives, cardanol-TMS and cardanol-APS (C_{TMS} and C_{APS}), were used as crosslinkers in the inverse vulcanisation reaction to generate the polysulfides (Fig. 1). A notable difference in colour can be observed between the three crosslinkers. Cardanol-APS is a similar dark pink colour to cardanol; however, it has a much higher viscosity due to the hydrolysis of Si–OMe to Si–OH and subsequent condensation to generate extra crosslinks (*i.e.* Si–O–Si bonds). Cardanol-TMS, on the other hand, exhibits an orange colour (Fig. S1†).

The ^{1}H NMR spectra of all cardanol-based crosslinkers show the characteristic peaks of the C=C bonds at 5.05, 5.30, and 5.80 ppm. In addition, the proton signals for the aromatic group are observed at 6.25, 6.45, and 7.30 ppm in all three (Fig. S2†). For cardanol-TMS, peaks corresponding to the TMS group, with an integration of 9, are observed at 0.26 ppm (Fig. 1, top, green). For cardanol-APS, the propyl CH_2 groups appear at 0.61, 1.31, and 2.68 ppm, each integrating to 2. We also observe a signal of protons of the amine group at 3.69 ppm (Fig. 1, middle, red). In cardanol, the hydroxy proton is detected at 4.63 ppm (Fig. 1, bottom, blue), a signal that is absent in the spectra of the two derivatives of cardanol, cardanol-APS and cardanol-TMS. This result is corroborated by FT-IR analysis with an absence of the characteristic O–H stretch at 3400 cm^{-1} (Fig. S3–S7†). Confirming the successful synthesis of cardanol-APS, a broad peak at *ca.* 3300 cm^{-1} corresponding to the amine N–H stretch, is observed in the FT-IR spectrum, along with a peak at 1160 cm^{-1} corresponding to the presence of Si–O–Si bonds (Fig. S4†). Moreover, in the spectrum of cardanol-TMS, a peak corresponding to the Si–O bond is observed at 838 cm^{-1} (Fig. S5†).

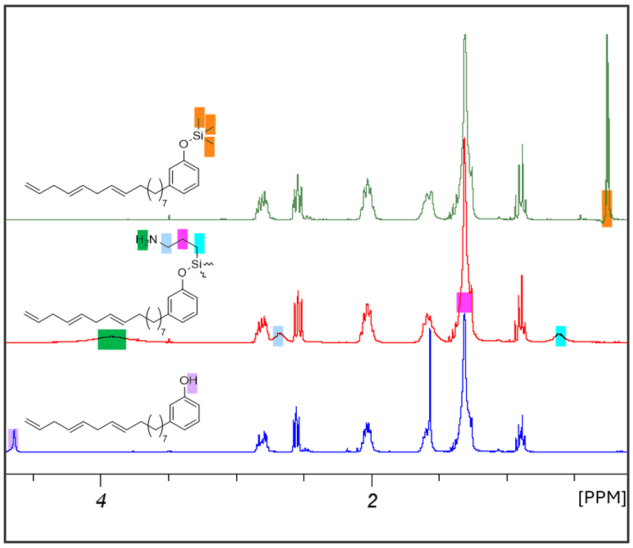

Fig. 1 ^{1}H NMR spectra of cardanol-based crosslinkers, C (blue, bottom), C_{APS} (red, middle) and C_{TMS} (green, top), in $CDCl_3$.

Synthesis and characterisation of polysulfides through inverse vulcanisation

Three polymers, poly-(S-*r*-C), poly-(S-*r*-C_{APS}), and poly-(S-*r*-C_{TMS}), were synthesised using a traditional inverse vulcanisation reaction at 180 °C with a 50 : 50 ratio of sulfur to cardanol-based crosslinker (Scheme 3 and Fig. S8–S12†). The resulting polysulfides exhibit a brown colour, with poly-(S-*r*-C_{APS}) observed at a lighter brown colour compared to the other two. In this polysulfide, the condensation that occurs during the synthesis of the crosslinker, cardanol-APS, leads to the formation of a Si–O–Si network, which contributes significantly to the degree of crosslinking (*e.g.*, both S–S and Si–O–Si links), leading to a substantially stronger material.

By comparing the FT-IR spectra of the three polysulfides, characteristic groups of each material are retained and identified as the O–H stretch at 3400 cm^{-1} in poly-(S-*r*-C) (Fig. 2, blue), the N–H stretch at 3330 cm^{-1} in poly-(S-*r*-C_{APS}) (Fig. 2, orange), accompanied by a peak at 1065 cm^{-1} for the Si–O–Si stretches, and a peak at 838 cm^{-1} for the Si–O stretch in poly-

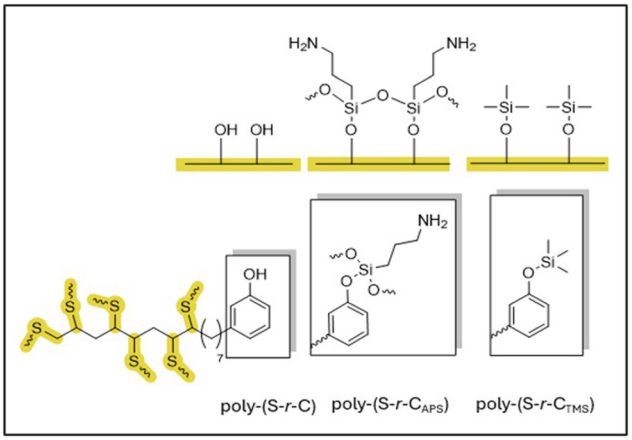

Scheme 3 Structures of the three synthesised polysulfides: poly-(S-*r*-C), poly-(S-*r*-C_{APS}), and poly-(S-*r*-C_{TMS}).

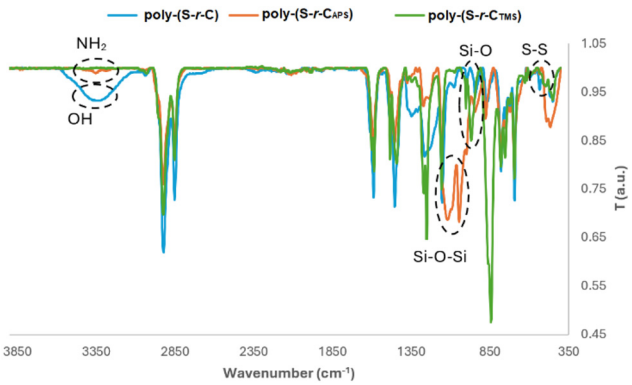

Fig. 2 FT-IR spectra of poly-(S-*r*-C) (blue), poly-(S-*r*-C_{APS}) (orange) and poly-(S-*r*-C_{TMS}) (green).

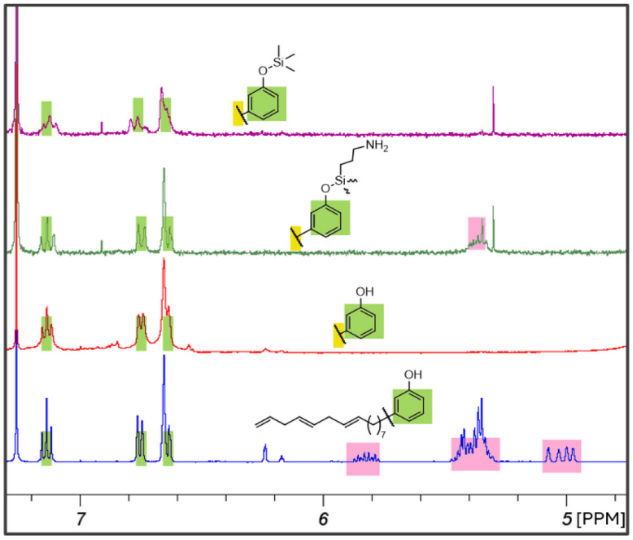

Fig. 3 Stacked ^{1}H NMR spectra of cardanol (blue), poly-(S-*r*-C) (red), poly-(S-*r*-C_{APS}) (green) and poly-(S-*r*-C_{TMS}) (purple), in $CDCl_3$.

(S-*r*-C_{TMS}) (Fig. 2, green).[24] The three polysulfides also show the characteristic S–S peak at 500 cm^{-1}.[25]

The comparison of ^{1}H NMR spectra of cardanol (Fig. 3, bottom, blue) and poly-(S-*r*-C) (Fig. 3, bottom middle, red) shows complete consumption of the alkene peaks (highlighted in pink), along with broadening in the polymer spectrum, consistent with network formation. The hydroxyl moiety on cardanol is observed in both FT-IR and ^{1}H NMR spectra of the poly-(S-*r*-C), indicating that the phenolic hydroxy is not lost during inverse vulcanisation, in contrast to the known behaviour of primary alcohols when subjected to the same reaction conditions (Fig. S11–S12†).[3,16]

Comparison of the ^{1}H NMR spectra of cardanol, poly-(S-*r*-C_{APS}) (Fig. 3, top middle, green and Fig. S9†), and poly-(S-*r*-C_{TMS}) (Fig. 3, top, purple and Fig. S8†) show that the inverse vulcanisation was successful as the alkene peaks at 5.05 and 5.80 ppm are no longer visible and the alkene signal at 5.30 ppm remains with reduced intensity. In the case of poly-(S-*r*-C_{APS}), the integration of peak 5.30 ppm decreases by 52%, relative to the aromatic signals (Fig. S10†), indicating that some alkene groups are left unreacted. This is due to the lower vitrification point of poly-(S-*r*-C_{APS}) after reacting with molten sulfur due to the presence of pre-formed Si–O–Si crosslinks. The early solidification prevents complete reaction of the alkene groups. Although the amine and propyl peaks are not clearly visible due to broadening, their presence is confirmed by FT-IR and ^{1}H–^{13}C HSQC NMR (Fig. 2 and S13†). For this polymer, this 2D NMR analysis suggests the presence of NH_2 functionalities, as a proton peak is observed that is not coupled to carbon atoms. This provides additional confidence in the presence of amine groups after polymerisation. However, we cannot fully rule out partial reactivity of the amine functionality during the inverse vulcanisation process, as previous studies have shown that primary amines can undergo complex reactions with elemental sulfur, potentially forming polysulfide species and releasing ammonia under certain conditions.[26] Despite the absence of evidence of such side reactions, amine and sulfur interactions cannot be excluded.

The successful incorporation of the trimethylsilyl-functionalised crosslinker and the progress of polymerisation was also investigated by comparing the ^{1}H NMR spectra of cardanol, cardanol-TMS, and the resulting poly-(S-*r*-C_{TMS}) (Fig. S8†). In the polysulfide spectrum, the alkene proton signals of cardanol-TMS at 5.05, 5.30, and 5.80 ppm are absent, confirming consumption of the alkene groups during inverse vulcanisation (Fig. 3). A signal at 0.25 ppm in the ^{1}H NMR spectrum corresponding to the trimethylsilyl (TMS) methyl protons, confirms incorporation of the hydrophobic silane functionality (Fig. S8†). The broadened peaks and reduced fine splitting in the polymer spectrum indicate restricted chain mobility, which may suggest some degree of crosslinking. However, since the polymers are soluble in several organic solvents, this points to the presence of linear or lightly branched structures rather than fully crosslinked networks. Recent work by Pyun

and co-workers has shown that inverse vulcanisation can produce a variety of architectures, linear, branched, or partially crosslinked, depending on the monomer structure and reaction conditions.[27]

Gel permeation chromatography analysis

To further understand polymer chain growth and molecular weight distribution, GPC analysis was performed on the synthesised polymers in THF. The unmodified cardanol polysulfide, poly-(S-*r*-C), showed a number average molecular weight (M_n) of approximately 14 000 Da ($Đ$ = 1.11), indicating a relatively narrow molecular weight distribution. While the functionalised materials poly-(S-*r*-C_{APS}) and poly-(S-*r*-C_{TMS}) showed significantly higher M_n values (between 118 to 121 kDa), suggesting successful chain growth during inverse vulcanisation. The C_{APS} monomer displayed a much lower M_n (approximately 2200 Da), confirming chain growth and polymer formation post-functionalisation (Fig. S14–S17†).

Coating and adhesion performance

The obtained polysulfides were tested as coatings on glass substrates (Fig. 4, top). Poly-(S-*r*-C) and poly-(S-*r*-C_{TMS}) were spin-coated onto the surface due to their lower viscosity, forming thin, homogeneous films. In contrast, poly-(S-*r*-C_{APS}) was directly applied to the glass using a spatula immediately after synthesis, as it was more viscous. Both poly-(S-*r*-C) and poly-(S-*r*-C_{TMS}) required some time to fully cure at room temperature, during which time, their shiny appearance gradually faded.

Adhesion was evaluated using the ASTM D3359 cross-hatch tape test.[28] A grid was cut into the polymer-coated glass substrates (Fig. 4, middle), and 3M adhesive tape was applied and subsequently peeled off to assess the integrity of the coatings (Fig. 4, bottom). Both poly-(S-*r*-C) and poly-(S-*r*-C_{APS}) showed excellent adhesion, with no visible material removal, indicating strong interaction with the glass surface and no interaction with the adhesive tape. In contrast, poly-(S-*r*-C_{TMS}) showed weaker adhesion, with partial delamination observed after tape removal. This difference reflects the influence of surface functionality: the polar hydroxy and amine groups in poly-(S-*r*-C) and poly-(S-*r*-C_{APS}) enhance adhesion, while the nonpolar trimethylsilyl group in poly-(S-*r*-C_{TMS}) limits effective interfacial bonding.

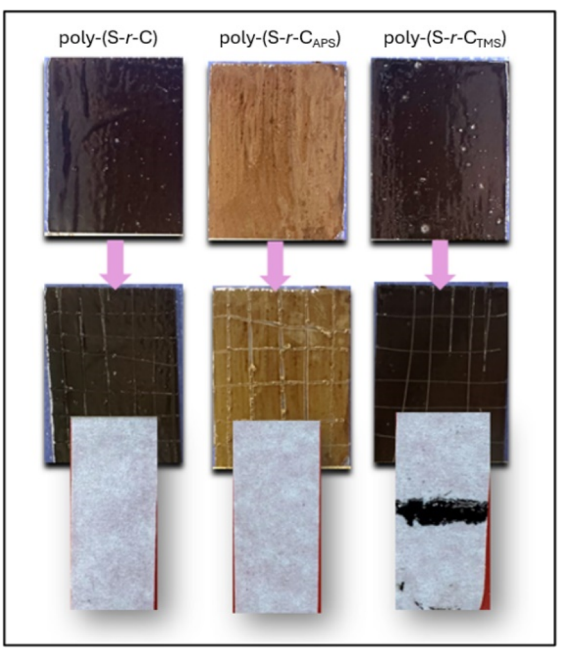

Fig. 4 Cross-hatch adhesion test (ASTM D3359) results for poly-(S-*r*-C), poly-(S-*r*-C_{APS}), and poly-(S-*r*-C_{TMS}) coatings on glass substrates (top), after cutting (middle), sticky side of 3M tape after test (bottom).

Physical properties

Contact angle measurements were carried out to assess the surface wettability of the samples and determine whether functionalisation influences the material's hydrophobicity. The hydrocarbon contact angles for all materials were measured as 0° when tested with hexane, decane, octane, mineral oil, silicone oil, and canola oil, indicating strong oleophilic behaviour. Upon droplet application, the liquids immediately spread across the material surface. For water contact angles, the values decreased over time until reaching a stable value. Based on the initial measurements, poly-(S-*r*-C_{TMS}) was the most hydrophobic, with an initial water contact angle of 95.12°, followed by poly-(S-*r*-C) at 87.89°, and poly-(S-*r*-C_{APS}) at 82.63° (Fig. S18†). This trend reflects the influence of surface functional groups: poly-(S-*r*-C_{TMS}) lacks polar moieties, while poly-(S-*r*-C) and poly-(S-*r*-C_{APS}) contain hydroxyl and amine groups, respectively, which increase surface polarity and water affinity. Overall, the materials exhibit good hydrophobicity, particularly poly-(S-*r*-C_{TMS}), but poor oleophobicity was observed across all samples.

Unsurprisingly, the solubility of the polysulfides in common solvents differ depending on the cardanol-based functional groups. All three polymers are soluble in toluene, THF, ethyl acetate, acetone, $CHCl_3$, DCM, and DMF but are insoluble in water (Table S1†). Poly-(S-*r*-C) is also soluble in ACN and ethanol but insoluble in methanol and hexane. In contrast, poly-(S-*r*-C_{APS}) is soluble in methanol and ethanol but insoluble in ACN and hexane, while poly-(S-*r*-C_{TMS}) is soluble in hexane but insoluble in ACN, methanol, and ethanol. This difference is due to the polarity of the functional groups: poly-(S-*r*-C) dissolves in polar solvents due to hydroxy groups, poly-(S-*r*-C_{APS}) in protic solvents due to the amine group, and poly-(S-*r*-C_{TMS}) in non-polar solvents due to hydrophobic silane groups.[29] Interestingly, even these small differences in functional groups lead to clear changes in solubility, allowing us to tailor the materials for specific applications, whether that's selecting the right solvent for applying coatings or making them easier to remove when needed.

Imaging

The three materials show a smooth surface by SEM (Fig. 5) and EDX analysis (Table S2†) confirmed the presence of all expected elements. For instance, nitrogen content, related to

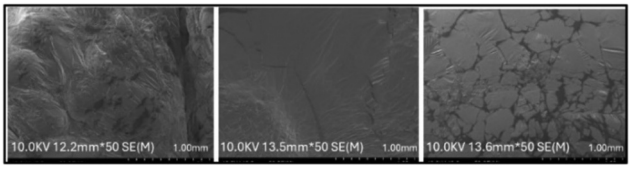

Fig. 5 SEM images of poly-(S-*r*-C), poly-(S-*r*-C_{APS}) and poly-(S-*r*-C_{TMS}) from left to right.

the presence of the amine group in poly-(S-*r*-C_{APS}), was 0.13%, and silicon atoms, present in both poly-(S-*r*-C_{APS}) and poly-(S-*r*-C_{TMS}), showed 3.7 and 4.3% values, respectively.

Thermal properties

TGA revealed extensive differences in thermal stability among the three surface-functionalised polysulfides (Fig. 6). The largest degradation onset was showed by poly-(S-*r*-C) at about 269 °C, with 22.8% of its original weight remaining at 700 °C (Fig. 6, blue, and Fig. S19†). This may be attributed to the hydroxyl functional groups that enable hydrogen bonding between polymer chains, providing enhanced thermal resistance and structural stiffness. Both poly-(S-*r*-C_{APS}) and poly-(S-*r*-C_{TMS}) initiated degradation around 238 °C but had very different thermal stabilities at high temperatures. Poly-(S-*r*-C_{APS}) retained 37.4% of its original mass (Fig. 6, grey, and Fig. S20†), whereas poly-(S-*r*-C_{TMS}) retained only 16.9% of its original mass at 700 °C (Fig. 6, orange, and Fig. S21†).

The higher residue for poly-(S-*r*-C_{APS}) arises from the formation of a heat-resistant Si–O–Si crosslinks which provide a more rigid and stable inorganic backbone. On the other hand, poly-(S-*r*-C_{TMS}) lacks such an extensive Si–O–Si connectivity. No crosslinking is contributed by the nonpolar Si–CH_3 groups, resulting in reduced thermal stability and lower char yield. These results highlight the influence of polarity and network topology on thermal behaviour: hydrogen bonding enhances the performance of poly-(S-*r*-C), siloxane network formation dominates in poly-(S-*r*-C_{APS}), and the limited interactions in poly-(S-*r*-C_{TMS}) lead to the lowest thermal residue.[30]

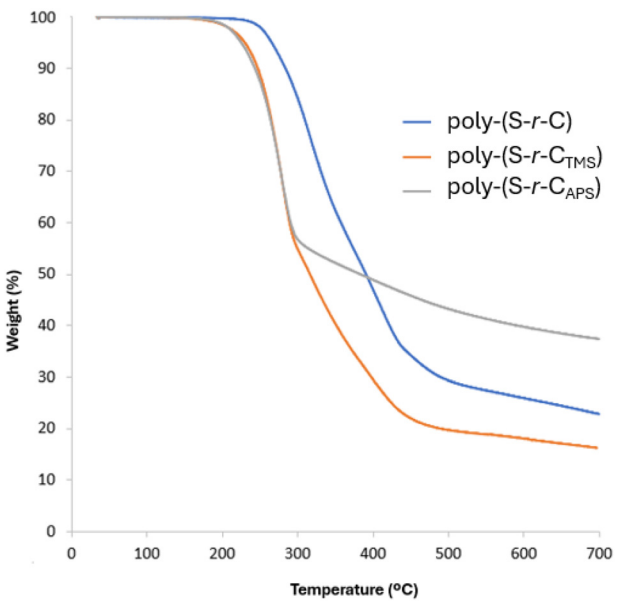

Fig. 6 Thermogravimetric analysis (TGA) curves of poly-(S-*r*-C) (blue), poly-(S-*r*-C_{APS}) (grey), and poly-(S-*r*-C_{TMS}) (orange).

The DSC revealed that the glass transition temperature (T_g) of poly-(S-*r*-C) is −11.9 °C (Fig. S22†), that of poly-(S-*r*-C_{APS}) is −10.7 °C (Fig. S23†), while poly-(S-*r*-C_{TMS}) shows a much lower T_g at −34 °C (Fig. S24†). An endothermic peak was observed around 112 °C for all three materials, corresponding to the melting temperature of elemental sulfur, indicating its presence. This peak disappeared in the second heating cycle as the sulfur was reincorporated into the material upon heating. Among the materials studied, the largest quantity of depolymerised sulfur is found in poly-(S-*r*-C_{APS}), due to the short reaction time, followed by poly-(S-*r*-C), and finally poly-(S-*r*-C_{TMS}), which contains the least. No exothermic peaks related to crystallisation were detected, confirming that all three materials remain amorphous between −75 °C and 150 °C.

These results suggest that the low T_g of poly-(S-*r*-C_{TMS}) is due to its hydrophobic trimethylsilyl groups, which enhance chain mobility and flexibility. In contrast, the higher T_g values of poly-(S-*r*-C) and poly-(S-*r*-C_{APS}) are attributed to hydrogen bonding from hydroxyl groups and amine groups in both, and the contribution of Si–O–Si and S–S network in poly-(S-*r*-C_{APS}) which restrict chain movement.

Conclusions

This work highlights the potential of using the renewable resource cardanol, and its functionalised derivatives, to create versatile sulfur-rich polymers through inverse vulcanisation. By modifying cardanol with different silane groups, we introduced tunable chemical functionalities that directly influence the physical, surface, and thermal properties of the resulting materials. The study shows that small changes in molecular structure such as adding polar or nonpolar groups, can significantly affect adhesion, flexibility, hydrophobicity, and thermal behaviour. These findings underline the importance of crosslinker modifications in developing sustainable materials with tuned properties and demonstrate that cardanol-based polysulfides are promising candidates for applications in coatings, adhesives, and beyond.

Author contributions

M. R. performed experimental work, characterisation and analysis, investigation, writing – original draft. M. L. assisted with experimental work, characterisation and analysis, investigation, writing – original draft. E. M. L. provided project conceptualisation, supervision, validation, and critical review & editing of the manuscript, funding acquisition.

Conflicts of interest

There are no conflicts to declare.

Data availability

The data for this article, including NMR and FTIR spectra, water contact angle images, solubility details, EDX data, and TGA and DSC thermograms, have been included as part of the ESI.†

Acknowledgements

This work was supported by the Royal Society Te Apārangi Marsden Grant (MFP-UOA2328). The authors would also like to thank the School of Chemical Sciences at the University of Auckland for financial and infrastructure support. We are grateful to Dr Yuan Tao for assistance with SEM.

References

1 C. V. Lopez, M. S. Karunarathna, M. K. Lauer, C. P. Maladeniya, T. Thiounn, E. D. Ackley and R. C. Smith, High Strength, Acid-Resistant Composites from Canola, Sunflower, or Linseed Oils: Influence of Triglyceride Unsaturation on Material Properties, *J. Polym. Sci.*, 2020, **58**(16), 2259–2266, DOI: **10.1002/pol.20200292**.

2 A. Nayeem, M. F. Ali and J. H. Shariffuddin, Polysulfide Synthesis Using Waste Cooking Palm Oil via Inverse Vulcanization, *Chem. Eng. Technol.*, 2022, **45**(5), 971–978, DOI: **10.1002/ceat.202100465**.

3 D. J. Parker, H. A. Jones, S. Petcher, L. Cervini, J. M. Griffin, R. Akhtar and T. Hasell, Low Cost and Renewable Sulfur-Polymers by Inverse Vulcanisation, and Their Potential for Mercury Capture, *J. Mater. Chem. A*, 2017, **5**(23), 11682–11692, DOI: **10.1039/C6TA09862B**.

4 Y. Zhang, F. Seidi, M. Ahmad, L. Zheng, L. Cheng, Y. Huang and H. Xiao, Green and Sustainable Natural Derived Polysulfides for a Broad Range of Applications, *Green Chem.*, 2023, **25**(17), 6515–6537, DOI: **10.1039/d3gc02005c**.

5 F. G. Müller, L. S. Lisboa and J. M. Chalker, Inverse Vulcanized Polymers for Sustainable Metal Remediation, *Adv. Sustainable Syst.*, 2023, **7**(5), 2300010, DOI: **10.1002/adsu.202300010**.

6 A. K. Mann, L. S. Lisboa, S. J. Tonkin, J. R. Gascooke, J. M. Chalker and C. T. Gibson, Modification of Polysulfide Surfaces with Low-Power Lasers, *Angew. Chem.*, 2024, **136**(23), e202404802, DOI: **10.1002/ange.202404802**.

7 J. M. Chalker, M. Mann, M. J. H. Worthington and L. J. Esdaile, Polymers Made by Inverse Vulcanization for Use as Mercury Sorbents, *Org. Mater.*, 2021, **03**(2), 362–373, DOI: **10.1055/a-1502-2611**.

8 A. Pirayesh, M. Salami-Kalajahi, H. Roghani-Mamaqani and F. Najafi, Polysulfide Polymers: Synthesis, Blending, Nanocomposites, and Applications, *Polym. Rev.*, 2019, **59**(1), 124–148, DOI: **10.1080/15583724.2018.1492616**.

9 A. Nayeem, M. F. Ali and J. H. Shariffuddin, Synthesis and Applications of Inverse Vulcanized Polysulfides from Bio-Crosslinkers, *Mater. Today: Proc.*, 2022, **57**, 1095–1100, DOI: **10.1016/j.matpr.2021.09.397**.

10 K. W. Park and E. M. Leitao, The Link to Polysulfides and Their Applications, *Chem. Commun.*, 2021, **57**(26), 3190–3202, DOI: **10.1039/d1cc00505g**.

11 W. J. Chung, J. J. Griebel, E. T. Kim, H. Yoon, A. G. Simmonds, H. J. Ji, P. T. Dirlam, R. S. Glass, J. J. Wie, N. A. Nguyen, B. W. Guralnick, J. Park, Á. Somogyi, P. Theato, M. E. Mackay, Y.-E. Sung, K. Char and J. Pyun, The Use of Elemental Sulfur as an Alternative Feedstock for Polymeric Materials, *Nat. Chem.*, 2013, **5**(6), 518–524, DOI: **10.1038/nchem.1624**.

12 T. Lee, P. T. Dirlam, J. T. Njardarson, R. S. Glass and J. Pyun, Polymerizations with Elemental Sulfur: From Petroleum Refining to Polymeric Materials, *J. Am. Chem. Soc.*, 2022, **144**(1), 5–22, DOI: **10.1021/jacs.1c09329**.

13 J. Pyun and R. A. Norwood, Infrared Plastic Optics and Photonic Devices Using Chalcogenide Hybrid Inorganic/Organic Polymers via Inverse Vulcanization of Elemental Sulfur, *Prog. Polym. Sci.*, 2024, **156**, 101865, DOI: **10.1016/j.progpolymsci.2024.101865**.

14 M. S. Karunarathna, M. K. Lauer, T. Thiounn, R. C. Smith and A. G. Tennyson, Valorisation of Waste to Yield Recyclable Composites of Elemental Sulfur and Lignin, *J. Mater. Chem. A*, 2019, **7**(26), 15683–15690, DOI: **10.1039/C9TA03222C**.

15 S. Shukla, A. Ghosh, U. K. Sen, P. K. Roy, S. Mitra and B. Lochab, Cardanol Benzoxazine-Sulfur Copolymers for Li-S Batteries: Symbiosis of Sustainability and Performance, *ChemistrySelect*, 2016, **1**(3), 594–600, DOI: **10.1002/slct.201600050**.

16 D. J. Parker, S. T. Chong and T. Hasell, Sustainable Inverse-Vulcanised Sulfur Polymers, *RSC Adv.*, 2018, **8**(49), 27892–27899, DOI: **10.1039/C8RA04446E**.

17 H. Weng, C. Scarlata and H. D. Roth, Electron Transfer Photochemistry of Geraniol and (E,E)-Farnesol. A Novel "Tandem", 1,5-Cyclization, Intramolecular Capture, *J. Am. Chem. Soc.*, 1996, **118**(45), 10947–10953, DOI: **10.1021/ja962206z**.

18 A. Hoefling, D. T. Nguyen, Y. J. Lee, S.-W. Song and P. Theato, A Sulfur–Eugenol Allyl Ether Copolymer: A Material Synthesized via Inverse Vulcanization from Renewable Resources and Its Application in Li–S Batteries, *Mater. Chem. Front.*, 2017, **1**(9), 1818–1822, DOI: **10.1039/C7QM00083A**.

19 S. Basiouni, N. Abel, W. Eisenreich, H. L. May-Simera and A. A. Shehata, Structural Analysis of Cardanol and Its Biological Activities on Human Keratinocyte Cells, *Metabolites*, 2025, **15**(2), 83, DOI: **10.3390/metabo15020083**.

20 Y.-H. Fu, Y. Zhang, F. Wang, L. Zhao, G.-B. Shen and X.-Q. Zhu, Quantitative Evaluation of the Actual Hydrogen Atom Donating Activities of O–H Bonds in Phenols: Structure–Activity Relationship, *RSC Adv.*, 2023, **13**(5), 3295–3305, DOI: **10.1039/D2RA06877J**.

21 Y. Gnanou and G. Hizal, Effect of Phenol and Derivatives on Atom Transfer Radical Polymerization in the Presence of Air, *J. Polym. Sci., Part A: Polym. Chem.*, 2004, **42**(2), 351–359, DOI: **10.1002/pola.11003**.

22 P. Jia, F. Song, Q. Li, H. Xia, M. Li, X. Shu and Y. Zhou, Recent Development of Cardanol Based Polymer Materials-A Review, *J. Renewable Mater.*, 2019, **7**(7), 601–619, DOI: **10.32604/jrm.2019.07011**.

23 C. Voirin, S. Caillol, N. V. Sadavarte, B. V. Tawade, B. Boutevin and P. P. Wadgaonkar, Functionalization of Cardanol: Towards Biobased Polymers and Additives, *Polym. Chem.*, 2014, **5**(9), 3142–3162, DOI: **10.1039/C3PY01194A**.

24 E. Pretsch, in *Structure Determination of Organic Compounds: Tables of Spectral Data*, Springer, Berlin, 5th edn, 2020. DOI: **10.1007/978-3-662-62439-5**.

25 C. N. R. Rao, R. Venkataraghavan and T. R. Kasturi, Contribution to the Infrared Spectra of Organosulphur Compounds, *Can. J. Chem.*, 1964, **42**(1), 36–42, DOI: **10.1139/v64-006**.

26 K. Mori and Y. Nakamura, Reaction of sulfur compounds activated by amines. II. Reaction of sulfur and some aliphatic primary amines, *ACS Publications*, 1971, DOI: **10.1021/jo00819a030**.

27 J. Bao, K. P. Martin, E. Cho, K.-S. Kang, R. S. Glass, V. Coropceanu, J.-L. Bredas, W. O. Parker, J. T. Njardarson and J. Pyun, On the Mechanism of the Inverse Vulcanization of Elemental Sulfur: Structural Characterization of Poly(Sulfur- *Random* -(1,3-Diisopropenylbenzene)), *J. Am. Chem. Soc.*, 2023, **145**(22), 12386–12397, DOI: **10.1021/jacs.3c03604**.

28 ASTM D3359 Test Methods For Measuring Adhesion By Tape - Micom. **https://www.micomlab.com/micom-testing/astm-d3359/** (accessed 2025-05-08).

29 C. Reichardt, *Solvents and Solvent Effects in Organic Chemistry*, Fourth, updated and enlarged edition, Wiley-VCH: Weinheim, 2011, DOI: **10.1002/9783527632220**.

30 S. Dreisch, C. Hernandez, J. Horn and S. Neuenfeld, Thermal Stability of Amine Compounds and Dichloromethane, *Chem. Eng. Trans.*, 2016, **48**, 763–768, DOI: **10.3303/CET1648128**.